ISSN: 2694-166X
Scientific Journal
Biology & Life Sciences
DOI: 10.33552/SJBLS.2025.03.000578
Iris Publishers

Review Article

Theoretical Investigation on Fe (III)- Catalyzed Reductive Radical Ring Ex-Pansion of Cyclopropenone and Olefins Leading to Pyrone and Indanone

Nan Lu* and Junling Duan

College of Chemistry and Material Science, Shandong Agricultural University, Taian 271018, P. R. China

***Corresponding author:** Nan Lu, College of Chemistry and Material Science, Shandong Agricultural University, Taian 271018, P. R. China

Received Date: March 07, 2025

Published Date: March 21, 2025

Abstract

The first theoretical investigation was provided by our DFT calculation on Fe(III)-catalyzed ring ex-pansion of cyclopropenone with 2-methyl-2-propen-1-ol and olefin. Fe catalyst is initially converted into Fe hydride species $Fe^{III}HLn$ assisted by silane and EtOH. Next, $Fe^{III}HLn$ transfers hydrogen atom to 2-methyl-2-propen-1-ol leading to alkyl radical, followed by conjugate Michael addition to diphenylcyclopropenone. Subsequently, single-electron transfer with Fe^{II} provides stable anion and regenerates Fe^{III}. Finally, the anion is protonated with EtOH and oxidized by air obtaining adduct, the dehydration of which generates desired product pyrone. Alternatively, when olefin is used as substrate, aldehyde is obtained without air oxidation. The own Friedel–Crafts acylation reaction is preferred yielding another product indanone. Comparatively, the concerted asynchronous dehydration and ring closure of last step is determined to be rate-limiting for Fe(III)-catalyzed ring expansion to pyrone. While the own Friedel–Crafts acylation is rate-limiting for indanone slightly unfavorable thermodynamically.

Keywords: Ring expansion; Fe(III); cyclopropenone; Friedel–Crafts acylation; dehydration

Introduction

As core structure of important natural products, the synthesis of pyrone has attracted attention of re-searchers such as Umemiya's synthesis of Fostriecin via enantioselective allylation of acetylenic aldehyde [1], Yang's synthesis of antitumor (−)-Pironetin by double hydroboration of allenes [2], McMullin's picea endophytes from Acadian [3] and Xu's low toxic CRM1 degrader [4]. In recent years, many efforts have been focused on efficient method under mild condition with cheap catalysts. There are still many shortcomings limiting the synthesis of these molecules. For example, expensive catalysts are demanded for enantioselective Heck arylation of acyclic olefins and Au-allenylidene promoted decarboxylative annulation [5,6]. Harsh condition exists in NHC-catalyzed [4 + 2] cycloaddition and atroposelective synthesis of triaryl α-pyranones [7,8]. Low yields are obtained in vinylogous synthesis of dihydropyranones and phosphine-catalyzed activation of cyclo-propenones in (3 + 2) annulation [9,10].

A versatile C3 synthon we are interested in is diphenylcyclopropenone as the smallest aromatic system in various transformations. With catalysis of organics, alkalis and transition metals, the cycloadditions are carried out in construction of heterocyclic skeletons. Ravikumar reported Palladium-catalyzed cascade C-C activation of cyclopropenone and carbonylative amination [11]. Li explored ring expansion strategy towards diverse azaheterocycles [12]. Sun developed Rh(III)-Catalyzed spiroannulation of ketimines with cyclopropenones via sequential C-H/C-C bond activation [13]. Wang realized Iron-catalyzed one-step synthesis of isothiazolone/1,2-selenazolone via [3+1+1] annulation of cyclopropenones [14]. On the other, reductive radical strategy is vital in C–C bond construction involving core hydrogen transfer. Gui gave practical olefin hydroamination with nitroarenes [15]. Qi completed reductive coupling of alkenes with unsaturated imines via radical pathway [16]. Gan summarized carbon quaternization of redox active esters by decarboxylative coupling and alkene hydrobenzylation mediated iterative outer-sphere steps [17,18]. There are also continuous progresses in Iron-catalyzed radical intermolecular addition and hydrogen atom transfer radical cyclization of alkenyl in-doles and pyrroles [19-21].

In this field, Wang group has made many contributions. The previous work includes iron(III)-catalyzed re-duction radical cascade reaction to naphthodihydrofuran, regioselective addition of azonaphthalenes to polysubstituted oxazolidinones and reduction radical tandem strategy to β-alkenyl valerolactones [22-24]. An-other breakthrough of this group was Fe(III)-catalyzed ring expansion of cyclopropenone with olefins via radicals [25]. Although novel 2H-pyrones and substituted 1-indanones were synthesized, how two products were constructed in divergent paths with different substrates? What's the transformation between initial Fe(III) and Fe hydride species? Why own Friedel–Crafts acylation reaction is preferred for olefins? How dehydration condensation and Friedel–Crafts acylation occur in competition? What's the function of Fe(III) in hydrogen atom transfer and radical tandem? To solve these puzzled problems in experiment, an in-depth theoretical study was necessary for this strategy.

Computational Details

The geometry optimizations were performed at the B3LYP/BSI level with the Gaussian 09 package [26,27]. The mixed basis set of LanL2DZ for Fe and 6-31G(d) for other non-metal atoms [28-32] was denoted as BSI. Different singlet and multiplet states were clarified with B3LYP and ROB3LYP approaches including Becke's three-parameter hybrid functional combined with Lee–Yang–Parr correction for correlation [33,34]. The nature of each structure was verified by performing harmonic vibrational frequency calculations. Intrinsic reaction coordinate (IRC) calculations were examined to confirm the right connections among key transition-states and corresponding reactants and products. Harmonic frequency calculations were carried out at the B3LYP/BSI level to gain zero-point vibrational energy (ZPVE) and thermodynamic corrections at 333 K and 1 atm for each structure in ethanol (EtOH). The solvation-corrected free energies were obtained at the B3LYP/6-311++G(d,p) (LanL2DZ for Fe) level by using integral equation formalism polarizable continuum model (IEFPCM) in Truhlar's "density" solvation model [35-37] on the B3LYP/BSI-optimized geometries.

As an efficient method of obtaining bond and lone pair of a molecule from modern ab initio wave functions, NBO procedure was performed with Natural bond orbital (NBO3.1) to characterize electronic properties and bonding orbital interactions [38,39]. The wave function analysis was provided using Multiwfn_3.7_dev package [40] including research on frontier molecular orbital (FMO) and Mayer bond order (MBO).

Results and Discussion

The mechanism was explored for Fe(III)-catalyzed ring expansion of cyclopropenone 1 with 2-methyl-2-propen-1-ol 2 and olefin 4 to access pyrone 3 and indanone 5 (Scheme 1). $Fe(acac)_3$ was selected here as model catalyst according to experiment. Illustrated by black arrow of Scheme 2, Fe catalyst is initially converted into Fe hydride species $Fe^{III}HLn$ assisted by silane $PhSiH_3$ and EtOH. Next, $Fe^{III}HLn$ transfers a hydrogen atom to acceptor 2-methyl-2-propen-1-ol 2 leading to intermediate alkyl radical, followed by its con-jugate addition to Michael acceptor diphenylcyclopropenone 1. Subsequently, single-electron transfer with Fe^{II} provides stable anion E and regenerates Fe^{III}. E is protonated with EtOH and oxidized by air obtaining ad-duct F. Finally, the dehydration of F generates desired product pyrone 3 (path A red arrow). Alternatively, when olefin 4 is used as substrate, aldehyde F1 is obtained via protonation of anionic E1 with EtOH not its counterpart F via air oxidation. Then the own Friedel–Crafts acylation reaction is preferred to occur yielding another product indanone 5 (path B blue arrow). Figure 1 listed schematic structures of optimized TSs in Scheme 2. Tables s1-s3 gave activation energy for all steps.

Table S1. Calculated relative energies (all in kcal mol^{-1}, relative to isolated species) for the ZPE-corrected Gibbs free energies (ΔG_{gas}), Gibbs free energies for all species in solution phase (ΔG_{sol}) at 333 K by B3LYP/6-311++G(d,p)//B3LYP/6-31G(d) method and difference between absolute energy.

Species	ΔG_{gas}	$\Delta G_{sol(EtOH)}$
B+PhSiH3+EtOH	0	0
i0-1	-96.22	-75.95
ts-i0	-89.33	-70.7
i0-2	-100.59	-76.35
A+2	0	0
i1	-78.4	-68.52
ts-i12	-64	-56.25
i2	-81.06	-82.64
A+2-B	0	0
C	-17.36	-21.46
A+2-B+1	0	0
i3	-89.58	-114.76
ts-i3D	-82.24	-110.67
D	-119.06	-143.25
E	-140.34	-163.65

E+EtOH	0	0
i4	-12.06	-1.02
ts-i45	2.84	6.27
i5	-11.12	-4.41
E+EtOH-EtO+[O]	0	0
F	-82.2	-123.69
ts-Fi6	-50.71	-97.56
i6	-93.38	-132.98
E+EtOH-EtO+[O]-H2O	0	0
3	-25.98	-31.54
A+4	0	0
in1	-74.25	-74.44
ts-in12	-70.07	-72.12
in2	-76.55	-87.82
A+4-B	0	0
C1	-16.44	-20.92
A+4-B+1	0	0
in3	-85.23	-118.29
ts-in3D1	-78.15	-111.93
D1	-116.47	-143.81
E1	-127.8	-158.82
E1+EtOH	0	0
in4	-7.74	2.73
ts-in45	11.35	17.82
in5	-1.71	2.97
E1+EtOH-EtO	0	0
F1	24.55	-6.88
ts-F1in6	58.13	19
in6	35.05	2.95
E1+EtOH-EtO-2H	0	0
5	9.25	4.55

Table S2: The activation energy (local barrier) (in kcal mol^{-1}) of all reactions in the gas, solution phase calculated with B3LYP/6-311++G(d,p)//B3LYP/6-31G(d) method.

TS	$\Delta G^{\neq}_{gas}$	$\Delta G^{\neq}_{sol}$
ts-i0 (81i)	6.9	5.3
ts-i12 (156i)	14.4	12.3
ts-i3D (422i)	7.3	4.1
ts-i45 (664i)	14.9	7.3
ts-Fi6 (530i)	31.5	26.1
ts-in12 (192i)	4.2	2.3
ts-in3D1 (455i)	7.1	6.4
ts-in45 (1076i)	19.1	15.1
ts-F1in6 (113i)	33.6	25.9

Table S3: Mayer bond order (MBO) of typical TSs.

	Fe···H1	H1···O1	O1···Si	
ts-i0	0.66	0.25	0.48	
	Fe···H1	H1···C1		

ts-i12	0.58	0.32		
	C2···C4	C4···C6		
ts-i3D	0.36	1.05		
	O2···H2	H2···C6		
ts-i45	0.16	0.67		
	C3···O3	C3···O4	O3···H2	H2···O4
ts-Fi6	0.22	0.28	0.21	0.66
	Fe···H1	H1···C1	C1···C2	
ts-in12	0.67	0.24	1.58	
	C2···C4	C4···C6		
ts-in3D1	0.27	1.03		
	O2···H2	H2···C6		
ts-in45	0.28	0.53		
	C6···C7			
ts-F1in6	0.21			

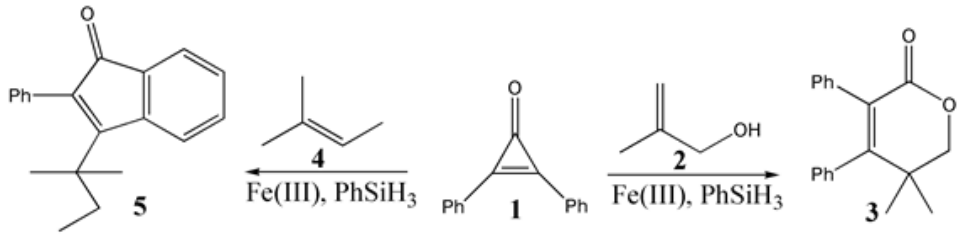

Scheme 1: Fe(III)-catalyzed ring expansion of cyclopropenone 1 with 2-methyl-2-propen-1-ol 2 and olefin 4 to access pyrone 3 and indanone 5.

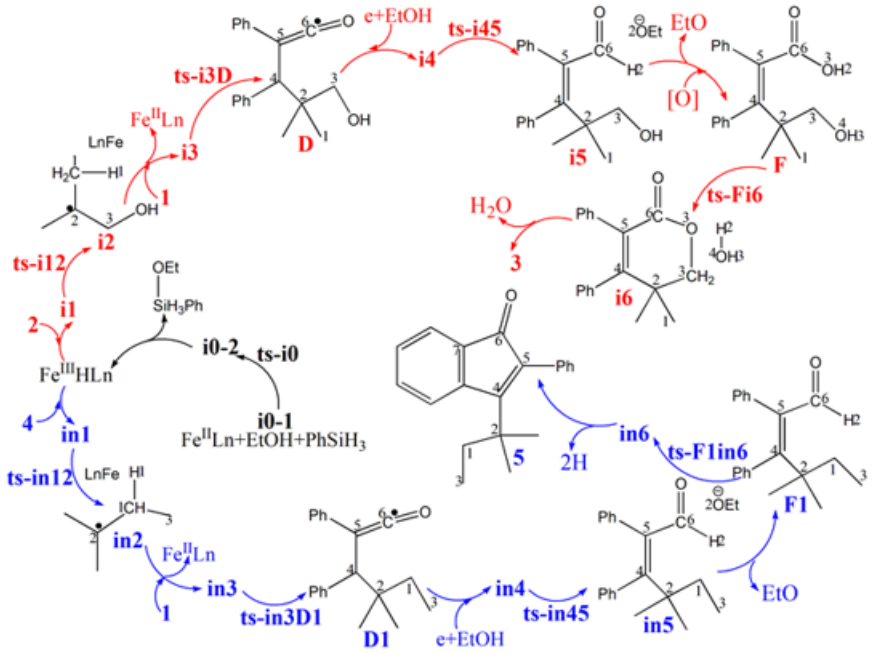

Scheme 2: Reaction mechanism of Fe(III)-catalyzed reductive radical ring expansion of 1 with 2 and 4 to access 3 and 5.

$Fe^{III}H$-Ln formation/H transfer/conjugate addition/protonation-oxidation/dehydration

Initially from complex i0-1 binding Fe catalyst, $PhSiH_3$ and EtOH, Fe catalyst is converted into Fe hydride species $Fe^{III}HLn$ via ts-i0 in step 1 with the activation energy of 5.3 kcal mol−1 exothermic slightly by -0.4 kcal mol^{-1} (black dash line of Figure 1a). The transition vector includes proton H1 shifting from O1 to Fe and cooperative linkage of O1-Si (2.18, 1.75 Å) suggesting proton capture of EtOH by $Fe^{III}Ln$ assisted by silane $PhSiH_3$. The i0-2 is obtained releasing reactive $Fe^{III}HLn$ after the removal of $EtO-SiH_3Ph$. The intermediate i1 is formed from substrate 2-methyl-2-propen-1-ol 2 with $Fe^{III}HLn$ in hand (red dash line of Figure 1a). The hydrogen atom H1 could be accepted by 2 via ts-i12 in step 2 with activation energy of 12.3 kcal mol^{-1} exothermic by -14.1 kcal mol^{-1} generating i2. The transition vector corresponds to proton transfer Fe···H1···C1 (1.76, 1.82 Å). Thus besides resultant $Fe^{II}Ln$, C1 of terminal alkene becomes sp3 hyprid methyl group $-CH_3$ together with new alkyl radical at C2 ready for the following step.

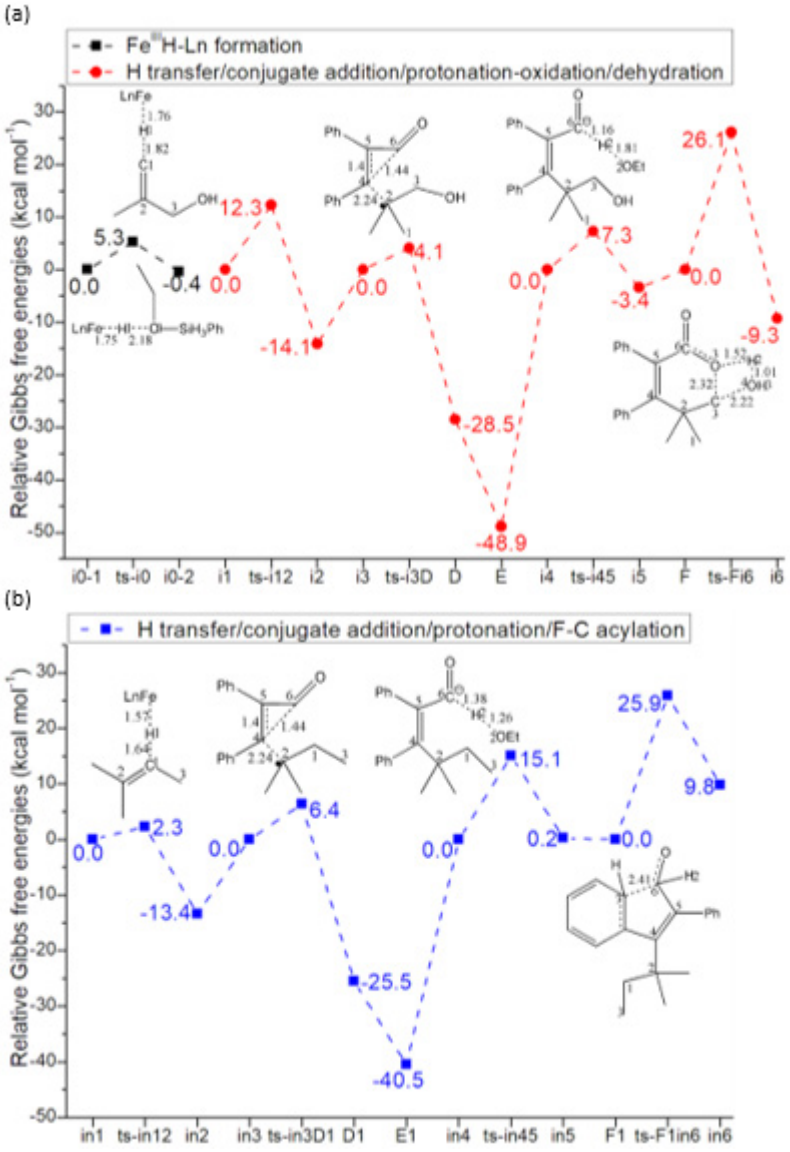

Figure 1: Relative Gibbs free energy profile in solvent phase starting from complex (a) i0-1, i1, i3, i4, F (b) in1, in3, in4, F1 (Bond lengths of optimized TSs in Å).

Next, alkyl radical and Michael acceptor diphenylcyclopropenone 1 assembles i3, from which the conjugate addition takes place via ts-i3D with activation energy of 4.1 kcal mol^{-1} affording the stable structure of accumulated diene D exothermic by -28.5 kcal mol^{-1}. The transition vector is about conjugate addition from C2 to C4 and resulting elongation of C4-C6 (2.24, 1.44 Å). As the single bond C2-C4 forms and the triple ring of 1 opens, the single electron is located at middle C6 of accumulated diene D which turns to be

anion E via single-electron transfer provided by Fe^{II} regenerating Fe^{III}. E is more stable than D with relative energy decreased by 20.4 kcal mol^{-1}. Subsequently with additional EtOH, E is protonated via ts-i45 in step 4 with activation energy of 7.3 kcal mol^{-1} with respect to i4 exothermic by -3.4 kcal mol^{-1} delivering intermediate i5. The transition vector corresponds to proton transfer from EtOH to anion C6 that is O2···H2···C6 (1.81, 1.16 Å). Evidently, the protonation of anion is readily accessible. Without EtO, aldehyde group in i5 is further oxidized by air through O3 insertion into C6-H2 generating carboxyl group in adduct F.

Finally, the dehydration of F happens via ts-Fi6 in step 5 with increased activation energy of 26.1 kcal mol^{-1} exothermic by -9.3 kcal mol^{-1} giving i6. The transition vector reveals typical concerted asynchronous step including detailed atomic motion about previous hydroxyl –O4H3 breaking down from C3, capture of H2 by O4 and later C3-O3 bonding, dissociation at O3-H2 (2.22, 1.01, 2.32, 1.52 Å) (Figure S1a). The desired product pyrone 3 is generated when the cyclic ester ring closure is completed along with leaving of newly formed water molecule H2O4H3. Comparatively, this complicated dehydration of last step 5 is determined to be rate-limiting for Fe(III)-catalyzed ring expansion producing pyrone.

H transfer/conjugate addition/protonation/Friedel–Crafts acylation

Alternatively, in1 is formed from substrate olefin 4 with $Fe^{III}HLn$ (blue dash line of Figure 1b). The hydrogen transfer proceeds via ts-in12 in step 2 with activation energy of 2.3 kcal mol^{-1} exothermic by -13.4 kcal mol^{-1} generating in2. The transition vector also contains Fe···H1···C1 (1.57, 1.64 Å) (Figure S1b). Here C1 of internal alkene becomes sp3 hyprid methylene group also with alkyl radical at C2. From in3 binding alkyl radical and 1, the conjugate Michael addition occurs via ts-in3D1 in step 3 with activation energy of 6.4 kcal mol^{-1} exothermic by -25.5 kcal mol^{-1} delivering intermediate D1. The transition vector also corresponds to SN2 attack of C2···C4···C6 (2.24, 1.44 Å) the same with ts-i3D. After single-electron transfer, anion E1 is also more stable than D1. The subsequent protonation with additional EtOH proceeds via ts-in45 in step 4 with activation energy of 15.1 kcal mol^{-1} endothermic unremarkably by 0.2 kcal mol^{-1} yielding in5. Releasing EtO, aldehyde F1 is obtained not like the case of counterpart F via air oxidation. The transition vector reveals proton transfer mode of O2···H2···C6 (1.26, 1.38 Å) (Figure S1c).

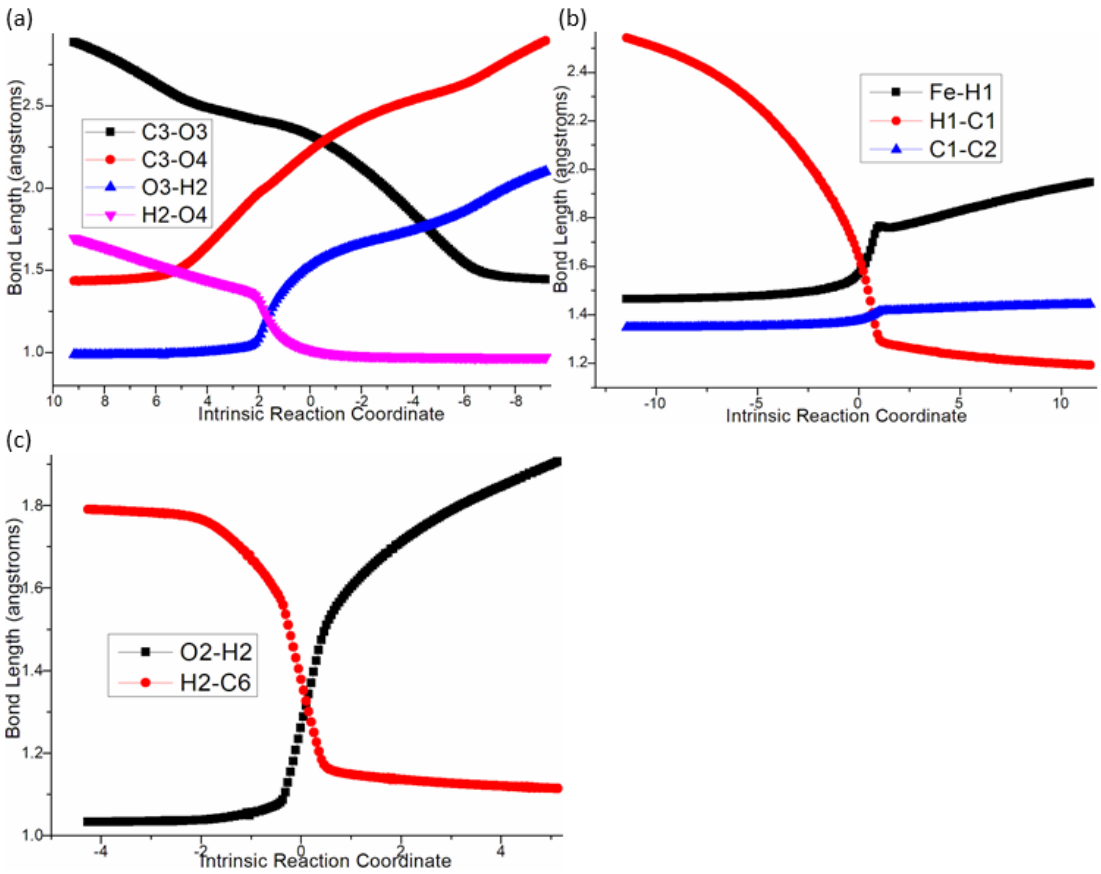

Figure S1: Evolution of bond lengths along the IRC for (a) ts-Fi6 (b) ts-in12 (c) ts-in45 at B3LYP/6-311++G(d,p) level.

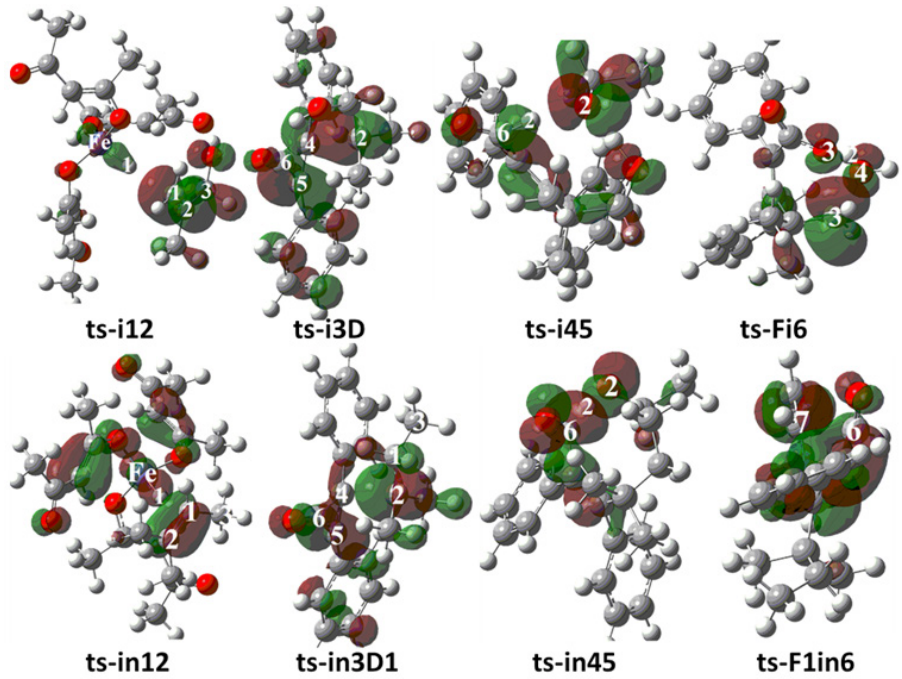

Figure S2: Highest Occupied Molecular Orbital (HOMO) of typical TSs. Different colors are used to identify the phase of the wave functions.

Then the own Friedel–Crafts acylation reaction is preferred from F1 via ts-F1in6 in step 5 with the activation energy of 25.9 kcal mol^{-1} endothermic by 9.8 kcal mol^{-1} realizing ring closure of in6. The transition vector demonstrates nucleophilic approach of C6 to C7 (2.24 Å). The bonding of C6-C7 makes C6 and C7 both sp3 hybrid thermodynamically unfavorable. Therefore it's easy to kick away two H atoms to recover sp2 hybrid obtaining another product indanone 5. The own Friedel–Crafts acylation of last step 5 is rate-limiting for Fe(III)-catalyzed ring expansion leading to indanone.

Conclusions

The first theoretical investigation was provided by our DFT calculation on Fe(III)-catalyzed ring expansion of cyclopropenone with 2-methyl-2-propen-1-ol and olefin. Fe catalyst is initially converted into Fe hydride species $Fe^{III}HLn$ assisted by silane $PhSiH_3$ and EtOH. Next, $Fe^{III}HLn$ transfers hydrogen atom to acceptor 2-methyl-2-propen-1-ol leading to alkyl radical intermediate, followed by its conjugate Michael addition to diphenylcyclopropenone. Subsequently, single-electron transfer with Fe^{II} provides much more stable anion and regenerates Fe^{III}. Finally, the anion is protonated with EtOH and oxidized by air obtaining adduct, the dehydration of which generates desired product pyrone. Alternatively, when olefin is used as substrate, aldehyde is obtained without air oxidation. The own Friedel–Crafts acylation reaction is preferred yielding another product indanone. Comparatively, the concerted asynchronous dehydration and ring closure of last step 5 is determined to be rate-limiting for Fe(III)-catalyzed ring expansion producing pyrone. While the own Friedel–Crafts acylation is rate-limiting for indanone slightly unfavorable in thermodynamics.

Electronic Supplementary Material

Supplementary data available: [Computation information and cartesian coordinates of stationary points; Calculated relative energies for the ZPE-corrected Gibbs free energies (ΔG_{gas}), and Gibbs free energies (ΔG_{sol}) for all species in solution phase at 333 K.]

Author contributions

Conceptualization, Nan Lu; Methodology, Nan Lu; Software, Nan Lu; Validation, Nan Lu; Formal Analysis, Nan Lu; Investigation, Nan Lu; Resources, Nan Lu; Data Curation, Nan Lu; Writing-Original Draft Preparation, Nan Lu; Writing-Review & Editing, Nan Lu; Visualization, Nan Lu; Supervision, Nan Lu; Project Administration, Nan Lu; Funding Acquisition, Junling Duan. All authors have read and agreed to the published version of the manuscript.

Funding

This work was supported by Key Laboratory of Agricultural Film Application of Ministry of Agriculture and Rural Affairs, P.R. China.

Conflict of Interest

The authors declare no conflict of interest.

References

1. Umemiya S, Terada M (2021) Catalytic Enantioselective Allylation of Acetylenic Aldehydes by Chiral Phosphoric Acid/Transition Metal Cooperative Catalysis: Formal Synthesis of Ostracon. Org Lett 23(9): 3767-3771.
2. Yang L, Kong LY, Gu Q, Shao SJ, Hong R, et al. (2021) Stereoselective Access to Polypropionates Expedited by the Double Hydroboration of Allenes: Total Synthesis of Antitumor (−)-Pirone tin. CCS Chemistry 3(2): 769-779.
3. McMullin D, Green B, Prince N, Tanney J, Miller J, et al. (2017) Natural Products of Picea Endophytes from the Acadian. J Nat Prod 80(5): 1475-1483.
4. Xu HW, Jia S, Liu M, Li X, Meng X, et al. (2020) low toxic CRM1 degrader: Synthesis and anti-proliferation on MGC803 and HGC27. Eur J Med Chem 206(5): 112708-112710.
5. Oliveira C, Pfalz A, Correia CRD (2015) Quaternary Stereo genic Centers through Enantioselective Heck Arylation of Acyclic Olefins with Aryldiazonium Salts: Application in a Concise Synthesis of (R)-Verapamil. Agnew. Chem Int Ed 54(47): 14036-14039.
6. Duan XL, Shi HT, Yury Song WZ (2024) Au-alinidine promoted decarboxylative annulation to access unsaturated γ-lactams/lactones. Chem Commun 60(29): 3926-3929.
7. Yan J, Shi KX, Zhao CT, Ding LY, Yang LM, et al. (2018) NHC-catalyzed [4 + 2] cycloaddition reactions for the synthesis of 3′-spirocyclic oxindoles via a C-F bond cleavage protocol. Chem Commun 54(13): 1567-1570.
8. Zhang SM, Li JB, Liang Z, Wei DH, Du D, et al. (2022) Atroposelective Synthesis of Triaryl α-Pyranoses with 1,2-Diaxes by N-Heterocyclic Carbene Organocatalytic. Agnew Chem Int Ed 61(52): 202212005-202212009.
9. Wittmann S, Martzel T, Truong CTP, Tofino M, Odier S, et al. (2021) Alkylidene Meldrum's Acids as Platforms for the Vinylogous Synthesis of Dihydropyran ones. Agnew Chem Int Ed 60(20): 11110-11114.
10. He X, Tang Y, Li J, Shen S, Lear MJ, et al. (2022) Phosphine-catalyzed activation of cyclopropenones: a versatile C3 synthon for (3 + 2) annulations with unsaturated electrophiles. Chem Sci 13(43): 12769-12775.
11. Ravikumar PC, Nanda T (2020) A Palladium-Catalyzed Cascade C-C Activation of Cyclopropenone and Carbonylative Amination: Easy Access to Highly Functionalized Maleimide Derivatives. Org Lett 2(4): 1368-1374.
12. Li R, Li B, Zhang H, Ju CW, Qin Y, et al. (2021) A ring expansion strategy towards diverse azaheterocycles. Nat Chem 13(10): 1006-1016.
13. Sun M, Hu H, Li BS, Xu JL, Sun W, et al. (2022) Rh (III)-Catalyzed Spiro annulation of ketoimines with cyclopropenones via sequential C-H/C-C bond activation. Chem Commun 58(30): 4743-4746.
14. Wang HC, Yan RL (2022) Iron-Catalyzed One-Step Synthesis of Isothiazolone/1,2-Selenazolone Derivatives via [3 + 1+1] Annulation of Cyclopropenones, Anilines, and Elemental Chalcogens. Adv Synth Catala 364(4): 715-719.
15. Gui J, Pan CM, Jin Y, Qin T, Lo J, et al. (2015) Organic chemistry Practical Olefin Hydroamination with Nitroarenes. Science 348(6237): 886-891.
16. Qi JF, Tang HB, Chen CW, Cui SL, Xu G, et al. (2019) Reductive coupling of alkenes with unsaturated imines via a radical pathway. Org Chem Front 6(15): 2760-2764.
17. Gan XC, Zhang B, Dao Na, Bi C, Poke M, et al. (2024) Carbon quaternization of redox active esters and olefins by decarboxylative coupling. Science 384(6691): 113-118.
18. Kong L, Gan X c, van der Puy Lovett V A, Sheni R A (2024) Alkene Hydro benzylation by a Single Catalyst That Mediates Iterative Outer-Sphere Steps. J Am Chem Soc 146(4): 2351-2357.
19. Saladrigas M, Puig J, Bonjoch J, Bradshaw B (2020) Iron-Catalyzed Radical Intermolecular Addition of Unbiased Alkenes to Aldehydes. Org Lett 22(20): 8111-8115.
20. Zhao XH, Liu XT, Shu PF, Yuan C, An XT, et al. (2023) Asymmetric Divergent Synthesis of Ent-Kaurene-, Ent-A tisane-, Ent-Beyerene-, Ent-Trachylobane-, and Ent-Gibberellin-type Diterpenoids. J Am Chem Soc 145(1): 311-321.
21. Gharpure SJ, Chavan RS, Narang SR (2024) Iron-Mediated Hydrogen Atom Transfer Radical Cyclization of Alkenyl Indoles and Pyrroles Gives Their Fused Derivatives: Total Synthesis of Brucellae E and H. Org Lett 26(22): 4583-4588.
22. Zhang H, Wang B, Xu H, Li FY, Wang JY, et al (2021) Synthesis of naphthodihydrofurans via an iron(III)-catalyzed reduction radical cascade reaction. Org Chem Front 8(21): 6019-6025.
23. Li FY, Wang B, Xu H, Xiao Y, Huang DW, et al (2023) Synthesis of Poly-substituted Oxazolidinones via Regioselective Addition of Azonaphthalenes. Org Chem Front 10(16): 4086-4091.
24. Li FY, Wang B, Xu H, Xiao Y, Huang DW, et al (2023) alAn Fe(III)-Catalyzed Reduction Radical Tandem Strategy to Access Poly-Substituted β-Alkenyl Valerolactones. Org Chem Front 10(6): 1551-1556.
25. Y Xiao, DW Huang, J Liao, B Wang, JY Wang, et al. (2025) Fe(III)-Catalyzed Ring Expansion of Cyclopropenone from Olefins via Radicals to Access Pyrone and Indanone Derivatives. Organic Letters 27(3): 814-820.
26. Frisch MJ, Trucks GW, Schlegel HB (2010) Gaussian 09 (Revision B.01), Gaussian, Inc., Wallingford CT, England.
27. Hay P J, Wadt W R (1985) Ab initio effective core potentials for molecular calculations-potentials for the transition-metal atoms Sc to Hg. J. Chem. Phys 82(1): 270-283.
28. Lv H, Han F, Wang N, Lu N, Song Z, et al. (2022) Ionic Liquid Catalyzed C-C Bond Formation for the Synthesis of Polysubstituted Olefins. Eur J Org Chem 2022(45): e202201222-e202201227.
29. Zhuang H, Lu N, Ji N, Han F, Miao C (2021) Bu_4NHSO4-Catalyzed Direct N-Allylation of Pyrazole and its Derivatives with Allylic Alcohols in Water: A Metal-free, Recyclable and Sustainable System. Advanced Synthesis & Catalysis 363(24): 5461-5472.
30. Lu N, Lan X, Miao C, Qian P (2020) Theoretical investigation on transformation of Cr(II) to Cr(V) complexes bearing tetra-NHC and group transfer reactivity. Int J Quantum Chem 120(18): e26340-e26345.
31. Lu N, Liang H, Qian P, Lan X, Miao C (2020) Theoretical investigation on the mechanism and enantioselectivity of organocatalytic asymmetric Povarov reactions of anilines and aldehydes. Int J Quantum Chem 121(8): e26574-e26579.
32. Lu N, Wang Y (2023) Alloy and Media Effects on the Ethanol Partial Oxidation Catalyzed by Bimetallic Pt6M (M= Co, Ni, Cu, Zn, Ru, Rh, Pd, Sn, Re, Ir, and Pt). Computational and Theoretical Chemistry 1228(8): 114252-114260.
33. Catellani M, Mealli C, Motti E, Paoli P, Perez Carreno E, et al. (2002) Palladium-Arene Interactions in Catalytic Intermediates: An Experimental and Theoretical Investigation of the Soft Rearrangement between η1 and η2 Coordination Modes. J AM CHEM SOC 124(16):4336-4346.
34. Marenich AV, Cramer CJ, Truhlar DG (2009) Universal Solvation Model Based on Solute Electron Density and on a Continuum Model of the Solvent Defined by the Bulk Dielectric Constant and Atomic Surface Tensions. J Phys Chem B 113(18): 6378–6396.
35. Tapia O (1992) Solvent effect theories: Quantum and classical formalisms and their applications in chemistry and biochemistry. J Math Chem 10(1): 139-181.
36. Tomasi J, Persico M (1994) Molecular Interactions in Solution: An Overview of Methods Based on Continuous Distributions of the Solvent. Chem Rev 94(1): 2027-2094.

37. Tomasi J, Mennucci B, Cammi R (2005) Quantum Mechanical Continuum Solvation Models. Chem Rev 105(8): 2999-3093.

38. Reed AE, Weinstock RB, Weinhold F (1985) Natural population analysis. J Chem Phys 83(2): 735-746.

39. Reed AE, Curtiss LA, Weinhold F (1988) Intermolecular interactions from a natural bond orbital donor-acceptor view point. Chem Rev 88(6): 899-926.

40. Lu T, Chen F (2012) Multiwfn: A multifunctional wavefunction analyzer. J Comput Chem 33(5): 580-592.